JOURNAL OF PROPULSION AND POWER
Vol. 19, No. 1, January–February 2003

Sonic Injection from Diamond-Shaped Orifices into a Supersonic Crossflow

Sadatake Tomioka*
National Aerospace Laboratory of Japan, Kakuda, Miyagi 981-1525, Japan
and
Lance S. Jacobsen† and Joseph A. Schetz‡
Virginia Polytechnic Institute and State University, Blacksburg, Virginia 24061-0203

The plume from a diamond-shaped, sonic injector orifice was studied experimentally in a Mach 3 crossflow. The structure of the plume, as well as the near injector flowfield, were examined by flow visualization techniques, and penetration height growth and maximum concentration decay were evaluated from aerothermodynamic probing measurements at two downstream stations. For the transverse injection, the jet-to-freestream dynamic pressure ratio was varied from 0.3 to 2.0. At lower dynamic pressure ratios, the plume from the diamond-shaped injector penetrated farther across the main flow compared to that from an equivalent circular injector, whereas an increase in the dynamic pressure ratio resulted in a deterioration of the plume's sharpness, and penetration of the plume became comparable to that from the circular injector. Angled injections were applied to the diamond-shaped orifice to enhance the penetration at a high dynamic pressure ratio of 2.0. Giving sweepback angle to the orifice was as effective as the case with circular injectors in enhancing the penetration. Adding a moderate yaw angle to the sweptback, diamond-shaped orifice resulted in greatly enhanced penetration, unlike the case with the circular injector. In all cases, the decay rate of the maximum concentration was almost insensitive to the orifice shape.

Nomenclature

A	=	cross-sectional area
C_d	=	discharge coefficient
D	=	diameter
D_{eff}	=	effective diameter, Eq. (4)
G	=	mass flow rate
H	=	penetration height
M	=	Mach number
P	=	pressure in plenum chamber
q	=	dynamic pressure
R_b	=	effective radius, Eq. (5)
T	=	total temperature
X, Y	=	streamwise location and spanwise location from injector center
Z	=	height from (tunnel lower) wall
α	=	injectant mass fraction
α_{mix}	=	injectant mass fraction deduced with modified mixing analogy, Eq. (2)
β	=	enthalpy deficit factor due to induced vorticity, Eq. (3)
δ	=	boundary-layer thickness

Subscripts

a	=	freestream
c	=	with unheated injection
h	=	with heated injection
j	=	injectant, injector
p	=	measured with in-stream probe
VC	=	center of vorticity effect extent

Introduction

IT is generally expected that the supersonic combustion ramjet (scramjet) engine will be the most efficient propulsion system in the hypersonic flight regime. Because the flow speed within the combustor remains supersonic, the residence time within the combustor will only be of the order of milliseconds. Thus, efficient penetration and mixing must be achieved within the short duration, and transverse fuel injection from the wall is an attractive arrangement. There are also other important applications of transverse jet injection into supersonic or hypersonic crossflows, such as reaction jets for vehicle control, thrust vector control in nozzles, and thermal protection systems.

Various injection configurations, including different shapes and alignments of the injectors, injector arrays, and auxiliary mixing enhancement devices, have been tested in attempts to attain better mixing capability.[1–10] Among the more successful was a wedge-shaped orifice having a wedge-shaped front half and a round-shaped back half, introduced by Barber et al.[5] By the avoidance of the occurrence of boundary-layer separation ahead of the injectant jet, the wedge-shaped injector showed better penetration than a conventional circular injector. However, the round-shaped back half was believed to cause separation in the wake of the jet, and the low-pressure condition within the separation region caused intensive disturbances. Thus, introducing a wedged-shape portion on the back half of an orifice maybe beneficial in attaining greater penetration, and that is the concept studied here.

The dynamic pressure of the jet was kept quite low in the study of the wedge-shaped injector to avoid rapid expansion of the jet plume becoming a large blockage to the supersonic flow.[5] As an example of high-pressure injection through lower-disturbance shape injectors, an elliptical transverse injector was introduced by Gruber et al.[6] to

Presented as Paper 2000-0088 and 2001-1762 at the AIAA Aerospace Sciences Meeting and Exhibit, Reno, NV, 11 January 2000 and Int'l Planes and Hypersonic Systems and Technology Conference, Kyoto, Japan, 24 April 2001; received 18 May 2001; revision received 20 May 2002; accepted for publication 12 September 2002.

*Senior Researcher, Ramjet Propulsion Center, Kakuda Space Propulsion Laboratory. Member AIAA.

†Graduate Assistant, Aerospace and Ocean Engineering Department; currently, Postdoctoral Research Engineer, U.S. Air Force Research Laboratory, Dayton, OH 5433-7251. Member AIAA.

‡Fred D. Durham Chair, Aerospace and Ocean Engineering Department. Fellow AIAA.

reduce the separation ahead of the jet for better penetration. In the dynamic pressure ratio (q_j/q_a) range of 1–3, they observed smaller separation regions ahead of the jet with the elliptical transverse injector compared to an equivalent circular transverse injector, but they found no large penetration advantage of the elliptical transverse injector. Their results suggest two aspects of lower-disturbance shaped injector research. First, these lower-disturbance shaped injectors, including the wedge-shaped injector, should be tested over a wider range of dynamic pressure ratios to understand the range of these ratios in which the shape effectiveness is valid. This information is important to determine the operation conditions of these low-disturbance shape injectors. Second, one should apply some techniques to enhance penetration in cases of high-pressure injection through these lower-disturbance shaped injectors. Shimura et al.[11] reported that the pressure within the supersonic combustor oscillated quite violently when heat release took place in a subscaled engine test.[4] This violent oscillation of the pressure field into which the jet is to be injected will cause instability and oscillation of the injection when the sonic condition at the injector orifice is violated. Therefore, for stable injection within the combustor over a wide range of flight conditions, higher dynamic pressure injection would be preferable.

Low downstream angled injection has been reported, both to reduce the separation ahead of the jet and to increase the jet penetration height compared to the case with the circular injectors.[6–10] McClinton[7] explained these effects by introducing an "effective dynamic pressure ratio" that increased with sweepback angle. Mays et al.[8] explained this effect as being a result of reduced "effective back pressure" and consequently increased "effective pressure ratio" due to weaker interaction in the case with larger sweepback angles. Both McClinton[7] and Mays et al.[8] noted that the substantially increased dynamic pressure ratio would result in less total pressure loss of the jet and in a greater penetration. On the other hand, close examination of the near injector flowfield showed that the initial penetration of the jets through sweptback injectors was less than that through the perpendicular injector, mainly due to a reduction in the perpendicular component of the jet momentum.[6,9] The streamwise vortices induced by the jet/freestream interaction might play a key role in filling the gap between these two contradictory facts.[3,6] Low angled injection combined with a yaw angle was found to decrease penetration, but to enhance mixing.[10] However, a jet injected through a sweptback injector with a yaw angle was expected to cause intensive streamwise vortices and to roll up the adjacent plume in the case with a circular injector array.[3]

In the present study, we introduce a diamond-shaped orifice having a wedge-shaped portion on both the front and back halves of the orifice as a modified version of the earlier wedge-shaped injector. Both heated and cold air are injected at sonic speed into a Mach 3 crossflow, and injectant concentration profiles are deduced through total temperature measurements and the modified mixing analogy in Ref. 12, which takes vorticity effects on the enthalpy field into account. Penatration height, penetration growth with downstream distance, and the maximum concentration decay of the jet plume are investigated. The modified mixing analogy also enables us to estimate the extent and intensity of the streamwise vortices, so that the interaction between the plume and the induced streamwise vortices are also examined.

In the first half of our study, the injector is oriented perpendicular and the dynamic pressure ratio is varied over a wide range ($q_j/q_a = 0.3$–2.0). We also vary the size of the injector (compared to the boundary-layer thickness) to investigate scale effects. The results are compared to those with an equivalent circular injector, which was tested at identical conditions. In the second half of our study, both sweepback angles and yaw angles are given to the diamond-shaped orifice and air is injected at a jet-to-freestream dynamic pressure ratio of 2.0.

Experimental Apparatus and Measurements

Experimental Apparatus

The injector was set in a Mach 3 wind-tunnel facility at Virginia Polytechnic Institute and State University. Figure 1 shows

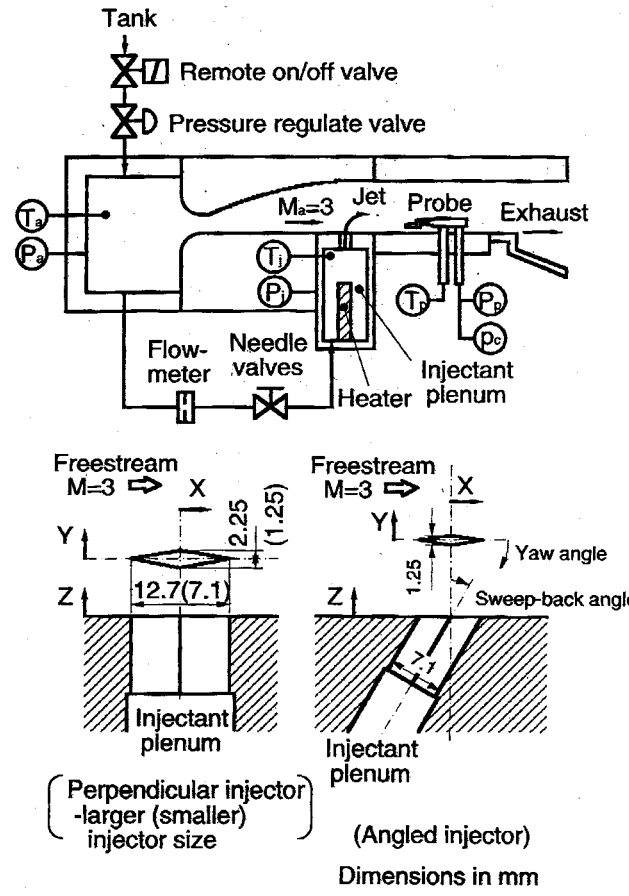

Fig. 1 Experimental apparatus and injector orifice configuration.

a schematic of the arrangement and the shape of the orifices. The facility is a blowdown-type tunnel, and a half-nozzle was installed to accelerate the airflow to Mach 3. The nozzle outlet area was 230 mm in width and 115 mm in height. The tunnel average plenum conditions were 620 kPa (P_a) and 285 K (T_a), which resulted in a freestream Reynolds number of 5.0×10^7/m. Test duration was typically 20 s. As shown in Fig. 1, we defined the X, Y, and Z coordinates in the streamwise direction, the spanwise direction, and the vertical direction, respectively, with a right-hand system and with the origin at the center of injector orifices. Figure 2 shows the Mach number and total temperature distributions in the boundary layer approaching the injector. The boundary layer and displacement thicknesses at the injector location were 8.5 and 3.3 mm, respectively.

Air was used as the injectant to simulate a high-molecular-weight gaseous hydrocarbon fuel injection. A portion of the air was bypassed from the tunnel plenum chamber to the injectant plenum chamber, so that the variation of the airflow total pressure is reflected in the injection pressure to maintain a constant dynamic pressure ratio. The injectant flow rate was controlled with a needle valve to attain the desired dynamic pressure ratio of the jet to the freestream (q_j/q_a) ranging from 0.3 to 2.0. The dynamic pressure ratios are kept within ±5% (±10% for $q_j/q_a = 0.3$) from desired values. Even at the lowest dynamic pressure ratio of 0.3, the jet-total-to-freestream-static pressure ratio ensured sonic injection. The injectant flow rate was measured with either a venturi flowmeter or an orifice flowmeter.

The injectant air was heated to produce a temperature difference between freestream and injectant, so that the mixing process could be documented through total temperature surveys downstream. We use the modified mixing analogy method in Ref. 12 to interpret these data. Two heaters and a copper heat sink with small holes were embedded in the plenum chamber of the injector, and the injectant was heated to about 380 K.

The diamond-shaped orifice had a half-angle of 10 deg on both its leading and trailing edges. Two injectors with different sizes were

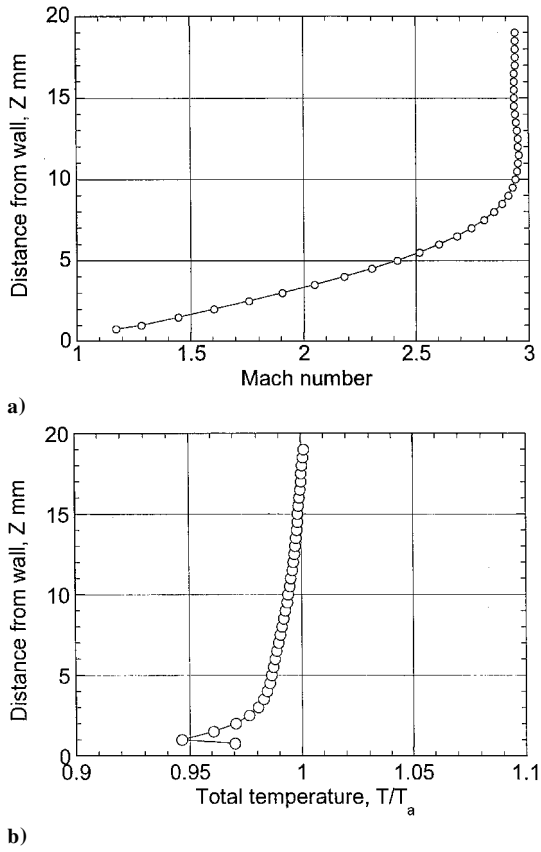

Fig. 2 Boundary-layer survey results: a) Mach number and b) total temperature (T_p normalized with freestream total temperature in plenum T_a) distributions.

used. The larger one had an equivalent diameter of 4.1 mm, and it was used for the perpendicular injection. Based on flow rate measurement, the effective equivalent diameter was 3.8 mm. The smaller injectors had an equivalent diameter of 2.4 mm, and they were used for both perpendicular and angled injections. Three injectors with sweepback angles of 0, 30, and 60 deg were used. Based on flow rate measurements, the effective equivalent diameters of these injectors were 2.3, 2.4, and 2.1 mm, respectively. This small effective diameter (and C_d) suggests that the boundary layer within the orifice hole made a throat within the orifice, and the jet could be accelerated to supersonic at the exit of the injector up to Mach 1.6, changing the jet-to-freestream dynamic pressure ratio. However, Cohen et al.[9] showed that the jet Mach number (1–2) has a small effect on initial penetration height (Mach disk height) normalized with the orifice exit diameter. Thus, in the present study, we assumed that the jet was issued from the orifice with the aforementioned effective area at the nominal ($M_j = 1$) condition. Yaw angles of 0, 15, and 30 deg were given to the 60-deg sweptback injector by rotating a block holding the injector.

To characterize the behavior of the plume from the diamond-shaped injector, one should have reference values of mixing-evaluation parameters such as the penetration height and its growth rate, as well as the maximum mass fraction and its decay rate, for direct comparisons. In the present study, we used an equivalent sonic circular injector perpendicular to the freestream as the reference case. The circular injector was equivalent in size to the larger diamond-shaped injector, whose effective diameter was measured as 4.2 mm.

Measurements and Data Reduction

Flow Visualization

Spark shadowgraphs were taken using a nanopulser with an exposure time of 2×10^{-8} s. Visualization of the surface flow patterns near the injector was accomplished via a use of 500 cS silicone oil with two different colors of fluorescent dye.

Pressure and Temperature Measurements

The pressure in the plenum chambers, P_a and P_j, was monitored by using pressure transducers, and the temperature in plenum chambers, T_a and T_j, was monitored by using type-E thermocouples. Data acquisition was performed with a personal computer and a 64-channel 16-bit A/D converter.

Total Temperature Probing

Aerothermodynamic measurements of the flowfield were taken 110 mm (designated as station 1) and 315 mm (designated as station 3) downstream from the center of the injector. A total temperature probe was used, which consisted of a tube with an o.d. of 1.59 mm and an i.d. of 1.04 mm. With three small holes drilled around the tube, the probe capture-to-recovery area ratio was 5 to 1. An exposed-junction type-E thermocouple with a bead of 0.25-mm diameter was placed inside the total temperature probe. This design can be expected to have a constant recovery factor over a wide range ($M = 1$–3) of Mach numbers.[13] Because the recovery factor is less than unity, the measured total temperature did not reach the plenum value in the freestream in the present experiments. A difference of 2–6 K was noted. This resulted in a recovery factor of 0.98 and a temperature measurement error of ±2 K. Even with a constant recovery factor of 0.98, the measured total temperature could differ from the true local value by 0.4% at $M = 1$ to 1.3% at $M = 3$. As shown in Ref. 12, the injectant mass fraction deduced through the modified mixing analogy method was insensitive to the recovery factor. Thus, no correction associated with the temperature recovery was made to the measured total temperature in the present study.

Modified Mixing Analogy

In a related study,[12] we modified the classical mixing analogy technique to take vorticity effects on the enthalpy field into account. This is essential in high-speed flows. We conducted both heated air injection (subscript h) and unheated air injection (subscript c). Assuming that the effects of the induced vorticity on the change in local enthalpy are proportional through a factor β (designated as "enthalpy deficit factor") to the local enthalpy and that both injectant mass concentration α and β are insensitive to the injectant temperature, we could describe the enthalpy balances as

$$(T_p)_h = (1-\beta)[(1-\alpha)(T_a)_h + \alpha(T_j)_h]$$
$$(T_p)_c = (1-\beta)[(1-\alpha)(T_a)_c + \alpha(T_j)_c] \quad (1)$$

Thus,

$$\alpha_{\text{mix}} = [(T_p/T_a)_h/(T_p/T_a)_c - 1]/\{(T_p/T_a)_h/(T_p/T_a)_c \times [1-(T_j/T_a)_c] - [1-(T_j/T_a)_h]\} \quad (2)$$

The validity of this modified mixing analogy was confirmed by comparison with direct measurements of injectant concentration using a tracer technique,[12] and it was found that the method is good enough to document the penetration height (determined as the height of the point with maximum injectant concentration in the present study) and the maximum concentration of the plume. See Ref. 12 for the details of the validation and error estimation. In brief, we expect a ±3% error at most in the injectant mass fraction. The major cause of the temperature measurement error was run-to-run scattering of the zero shift on the temperature measurement system. Thus, the temperature measurement error within each run would be smaller than the run-to-run error. Hence, the determination of the maximum injectant mass fraction location would be more reliable than that of the more conventional 5% injectant mass fraction location, and we used the height of the maximum concentration location from the tunnel wall as the penetration height of the plume, H. The repeatability of the maximum α_{mix} was within ±2%, and that of the penetration height was within ±0.5 mm.

From Eq. (1), we can also derive the enthalpy deficit factor as

$$\beta = 1 - (T_p/T_a)_h/[(1-\alpha_{\text{mix}}) + \alpha_{\text{mix}}(T_j/T_a)_h] \quad (3)$$

A feature of this technique is that it enables us to estimate the vorticity effects. Note that this factor is not correlated with vorticity quantitatively. However, we can make a qualitative comparison of the extent and relative intensity of the vorticity through the enthalpy deficit factor from different injectors.

Results and Discussion

Perpendicular Injection at Various Dynamic Pressure Ratios

In this section, the jet was injected perpendicular to the freestream. First, the basic characteristics of the diamond-shaped injector were examined over a wide range of dynamic pressure ratios ($q_j/q_a = 0.3$–2.0).

Flow Visualization

Figures 3a and 3b show shadowgraph images of the jet injected through the diamond-shape injector into quiescent air at a jet-static-to-ambient pressure ratio of 3.8. Clearly, the jet plume is turbulent. Figure 3a shows the plume looking at the long axis of the injector, and Fig. 3b shows the plume looking at the short axis. As shown in Fig. 3b, the plume expanded rapidly in the spanwise direction, and it showed the features of an overexpanded jet in Fig. 3a. This uneven expansion phenomenon has been reported as "axis switching" of the jet issuing from the elliptical orifice into quiescent,[14] coflowing,[15] and supersonic crossflow[6] environments. Thus, the original sharp diamond shape became a blunt diamond shape in the plume due to the uneven expansion, which would cause more disturbances in the freestream in the presence of a crossflow.

Figure 4 shows the variation of the Mach disk height of the jet injected into quiescent air vs the jet static to ambient pressure ratio. The height was normalized by the effective equivalent diameter.

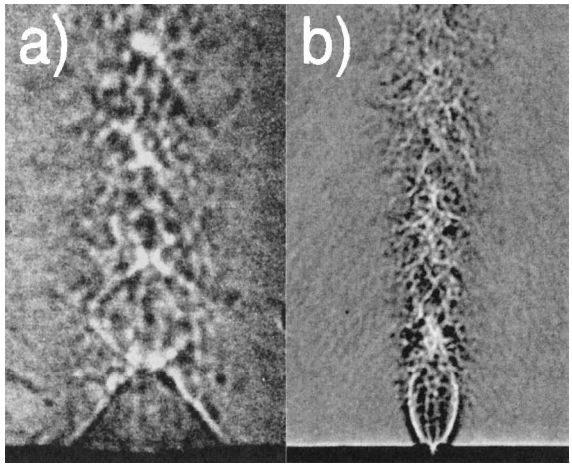

Fig. 3 Shadowgraphs of diamond-shaped jet injected into quiescent air.

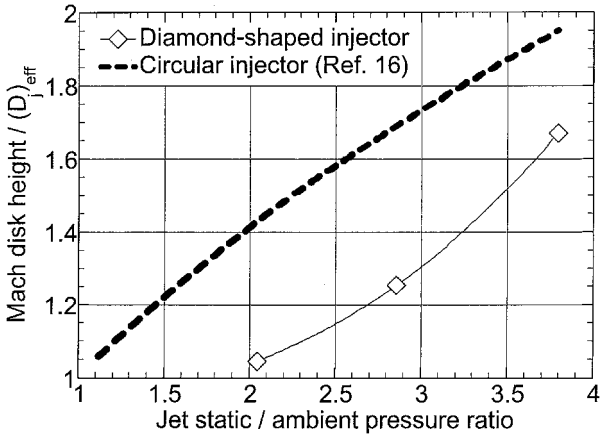

Fig. 4 Variation of Mach disk height with pressure ratio for quiescent background.

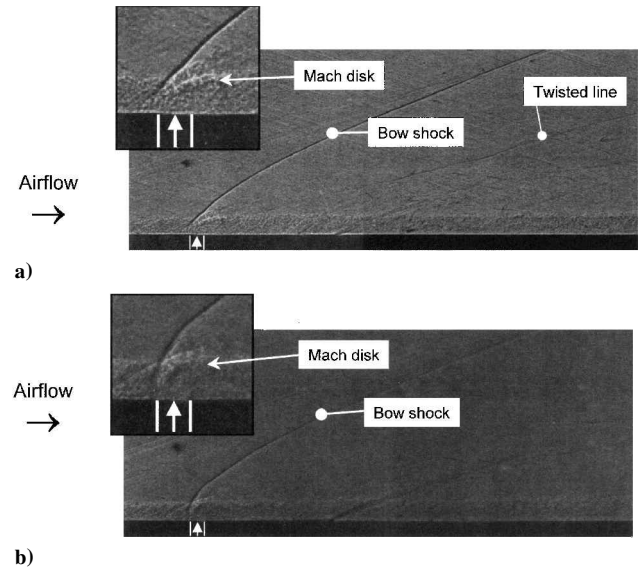

Fig. 5 Shadowgraph of jet injected into supersonic crossflow through a) diamond-shaped injector and b) circular injector at $q_j/q_a = 2.0$.

For comparison, the variation for a circular injector[16] is also shown in Fig. 4. The Mach disk height for the diamond-shaped injector is smaller than that from a circular injector, probably due to the uneven expansion.

Figure 5a shows a shadowgraph of the jet plume from the diamond-shaped injector interacting with the Mach 3 supersonic crossflow at $q_j/q_a = 2.0$. In Fig. 5a, the long axis of the injector is aligned with the external flow, and the freestream flow is from left to right. Figure 5b shows a shadowgraph of the jet plume from the circular injector at identical conditions. In both cases, barrel-like shocks and a Mack disk in the plume are visible near the injector. The barrel shocks are inclined downstream, showing strong interactions between the jet and the freestream, even in the case with injection from the diamond-shaped injector. The jet from the diamond-shaped injector expanded rapidly in the spanwise direction and became a bigger, blunter obstacle to the freestream with increasing q_j/q_a. Thus, a higher q_j/q_a might reduce the effectiveness of the diamond shape of the injector. Because of this strong interaction, a bow shock is visible ahead of the jet and rising up to the right. Note that the Mach disk height is somewhat larger with the circular injector than with the diamond-shaped injector, consequently, the bow shock is stronger with the circular injector. In turn, the separation ahead of the jet is much smaller with the diamond-shaped injector. In the case with the diamond-shaped injector, a twisted line is visible from the downstream triple point of the Mach disk and the barrel shocks, penetrating into the freestream with an angle less than the Mach angle in a $M = 3$ freestream. This line could be due to streamwise vortex motion, which will be discussed later. This line is not obvious in the case with the circular injector, though generation of streamwise vortices has been reported in many studies, for example, Ref. 17.

Figure 6 shows oil-flow surface patterns at various dynamic pressure ratios with both the diamond-shaped injector and the circular injector. The freestream flow is from left to right. In the case with the diamond-shaped injector, a separation occurred ahead of the jet at $q_j/q_a = 2.0$ because the jet expanded rapidly to form a blunt obstacle against the freestream. This interaction caused a rather strong bow shock ahead of the jet, which, in turn, resulted in a high effective backpressure condition for the jet. Note that the bow shock trace on the surface was stronger with the diamond-shaped injector than with the circular injector, in contrast to the impression one gets from the shadowgraphs. The uneven expansion of the jet in the spanwise direction from the diamond-shaped injector made this obstacle against the freestream shorter and wider than that in the case with the circular injector, resulting in this apparant discrepancy.

A very complicated secondary-flow pattern was observed in the jet wake in both cases at $q_j/q_a = 2.0$. Triangular accumulations of oil show the origin of a pair of streamwise vortices, which traveled

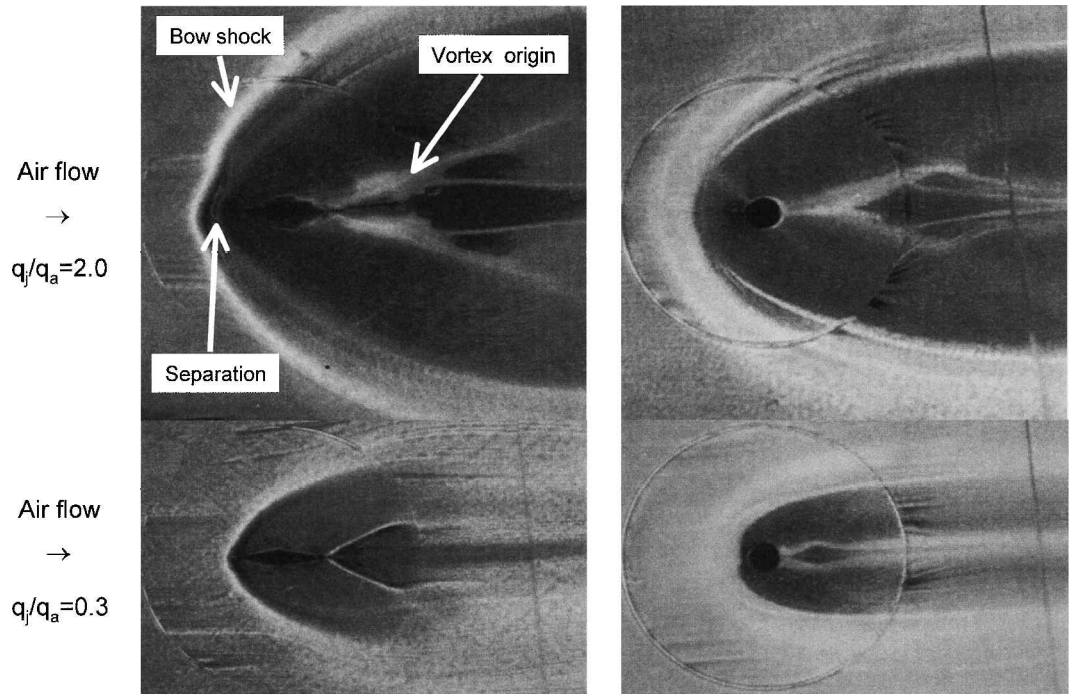

Fig. 6 Oil-flow visualization of surface flow with injection through a) diamond-shaped injector and b) circular injector at q_j/q_a = 2.0 and 0.3.

downstream. Though not clear in this still picture, the accumulations were observed to form half-cone shapes during the tunnel run. The jet expanded rapidly and turned the local freestream downward toward the wall, causing the streamwise vortices. With reduced dynamic pressure ratios of 1.0 and 0.5, the features of the flow pattern were almost identical, but with less intensity of interaction in both cases.

At $q_j/q_a = 0.3$, the separation ahead of the jet, secondary-flow patterns around the injector, and the oil accumulation in the jet wake disappeared in the case with the diamond-shaped injector, though they were still visible in the case with the circular injector. At this lower pressure ratio, the jet static pressure at the exit of the diamond-shaped orifice was close to the static pressure on an imaginary solid wedge surface with a wedge angle identical to that of the injector orifice (10 deg). Thus, the jet was in a "matched pressure" condition, and it caused a lesser disturbance to the freestream than in the higher-pressure ratio cases. This lesser disturbance might result in higher initial penetration. However, the flow pattern in the wake of the jet from the diamond-shaped injector showed that the streamwise vortex was also weakened, which might result in a reduction of mixing in the far field.

Injectant Contours

Figures 7a and 7b show contours of deduced injectant mass fraction with the diamond-shaped injector and the circular injector, respectively, with $q_j/q_a = 2.0$ at station 1. In both cases, the contours show mushroomlike shapes, having maximum concentration locations within the plume core above the boundary layer. The mushroomlike shape was more obvious with the circular injector, and more injectant was entrained into boundary layer in the case with the diamond-shaped injector. As shown in Fig. 6, the jet through the diamond-shaped injector expanded rapidly in the spanwise direction, and that permitted a larger portion of the injectant to be entrained into the boundary layer compared to the case with the circular injector. This uneven expansion also resulted in slightly less initial penetration (Mach disk height) of the jet from the diamond-shaped injector than in the case with the circular injector, which was observed earlier in Fig. 4. Note that the center of the plume is displaced slightly from the tunnel centerline in both cases. This

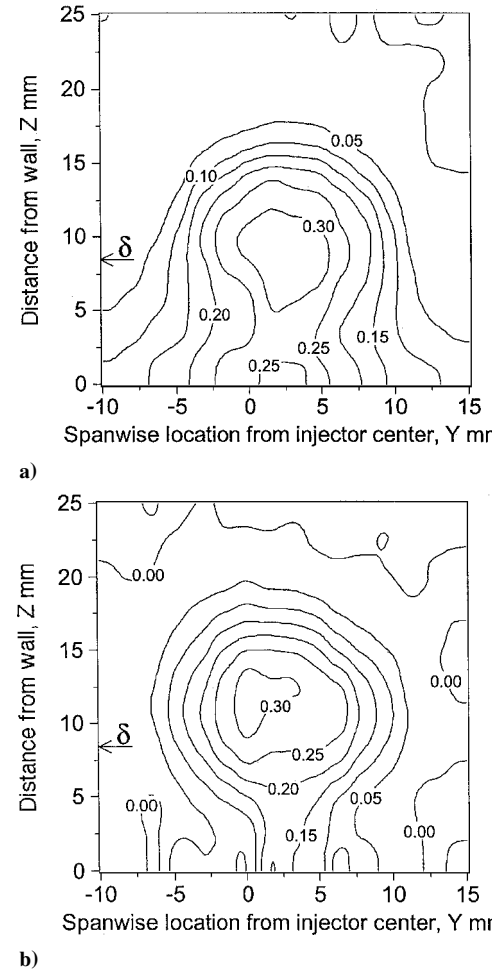

Fig. 7 Deduced injectant mass fraction (α_{mix}) contours with a) diamond-shaped injector and b) circular injector at q_j/q_a = 2.0 and at station 1 (X = 110 mm).

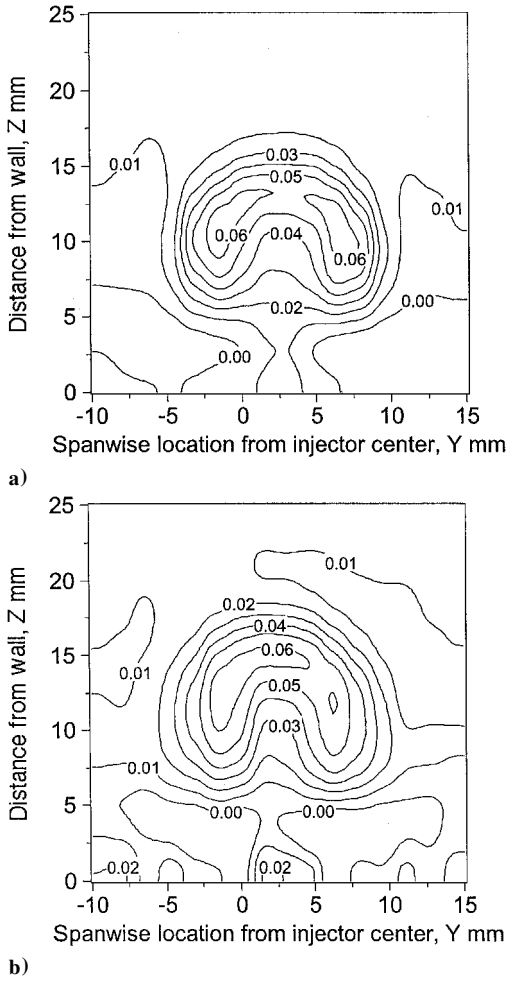

Fig. 8 Enthalpy deficit factor contours with a) diamond-shaped injector and b) circular injector at q_j/q_a = 2.0 and at station 1 (X = 110 mm).

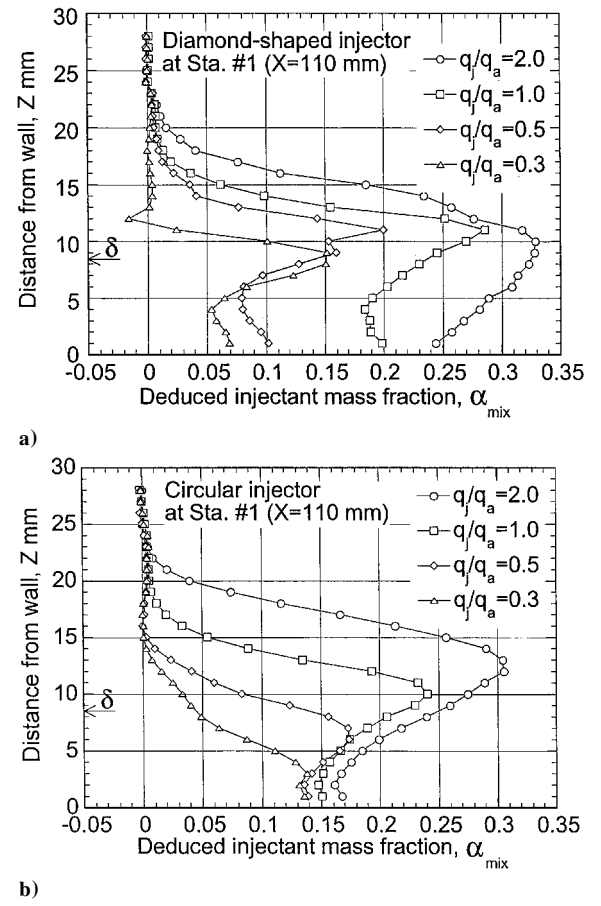

Fig. 9 Deduced injectant mass fraction (α_{mix}) distributions on contour symmetry plane at station 1 (X = 110 mm) with a) diamond-shaped injector and b) circular injector.

displacement was observed regardless of the injector configurations (for example, Ref. 4) and injection conditions, for example, low q_j/q_a with wedge-shaped injector in Ref. 5 and high q_j/q_a in Fig. 7a. The contour symmetry plane is located at about $Y = 2.0$–3.0 mm. Because the measurements were done at $Y = 1.6$ and 3.2 mm, distributions at $Y = 3.2$ mm were regarded as being on the symmetry plane in the present study. The contours of the jet plume through both injectors were still mushroomlike shapes at station 3, having maximum concentration locations within the plume core above the boundary layer.

Figures 8a and 8b show contours of the enthalpy deficit factor [Eq. (3)] with the diamond-shaped injector and the circular injector, respectively, with $q_j/q_a = 2.0$ at station 1. The presence of a pair of streamwise vortices is clearly shown in both cases. These vortices originated at the trailing edge of the injector as shown in Fig. 6. The vorticity effects are also indicated on the symmetry plane. Smaller vortices or longitudinal vortices would be present atop the plume. The streamwise vortices penetrated a little bit further in the case with the circular injector.

Jet Penetration Growth and Maximum Concentration Decay

Because the penetration of the plume is one of the main concerns in the present study, only the distributions on the contour symmetry plane will be shown in the following material.

Figures 9a and 9b show α_{mix} distributions on the contour symmetry plane with various dynamic pressure ratios at station 1 with the diamond-shaped injector and the circular injector, respectively. One can see that the penetration height with the diamond-shaped injector was not greatly affected by the dynamic pressure ratio, whereas that with the circular injector was obviously a strong function of the dynamic pressure ratio. At lower dynamic pressure ratios ($q_j/q_a = 0.5$ and 0.3), a considerable portion of the injectant was trapped in the boundary layer in the case with the circular injector, whereas a major portion of the injectant penetrated the boundary layer with the diamond-shaped injector. At higher dynamic pressure ratios, the behavior of the plumes is quite similar in the cases with both the diamond-shaped injector and the circular injector.

Figures 10a and 10b show α_{mix} distributions on the contour symmetry plane with various dynamic pressure ratios further downstream at station 3 with the diamond-shaped injector and the circular injector, respectively. With the circular injector, the penetration height decreased rapidly with decreasing the dynamic pressure ratio, and the plume core became indistinguishable at lower dynamic pressure ratios. However, the plumes from the diamond-shaped injector still had a clear core at station 3.

The penetration heights and maximum concentrations are summarized in Table 1, in which the penetration height was normalized with the effective diameter D_{eff} defined as

$$D_{eff} = (4A_j/\pi C_d)^{\frac{1}{2}} \tag{4}$$

where A_j is injector orifice area and C_d is the discharge coefficient. Injection at different dynamic pressure ratios through an identical orifice result in different injectant flow rates. In engine design, the limiting factor is total fuel flow rate, so that one would use a larger injector for lower q_j/q_a to attain an identical injectant flow rate. Thus, we should normalize both the height and the streamwise distance from the injector with a length scale in which injectant flow rates are taken into account to discuss the penetration height growth and maximum mass fraction decay. Barber et al.[5] introduced the effective radius in Ref. 18 to summarize the penetration data for different shaped injectors. The effective radius (R_b) is defined as[18]

$$R_b = (G_j/\rho_a V_a)^{\frac{1}{2}} \tag{5}$$

Table 1 Summary of penetration height and maximum injectant mass fraction of the jet plume with perpendicular injection (D_{eff}, in millimeters)

		Station 1				Station 3			
q_i/q_a	R_b, mm	X/R_b	H/D_{eff}	H/R_b	$\alpha_{\max}$	X/R_b	H/D_{eff}	H/R_b	$\alpha_{\max}$
				Diamond shaped (3.8)					
2.0	7.2	15.3	2.6 ± 0.1	1.4 ± 0.1	0.33 ± 0.03	43.7	4.0 ± 0.1	2.1 ± 0.1	0.16 ± 0.03
1.0	5.1	21.6	2.9 ± 0.1	2.2 ± 0.1	0.29 ± 0.03	61.8	3.7 ± 0.1	2.7 ± 0.1	0.09 ± 0.03
0.5	3.6	30.5	2.9 ± 0.1	3.1 ± 0.1	0.20 ± 0.03	87.4	3.7 ± 0.1	3.9 ± 0.1	0.06 ± 0.03
0.3	2.8	39.4	2.4 ± 0.1	3.2 ± 0.2	0.15 ± 0.03	112.3	3.4 ± 0.1	4.7 ± 0.2	0.03 ± 0.03
				Circular (4.2)					
2.0	8.1	13.7	2.8 ± 0.1	1.5 ± 0.1	0.31 ± 0.03	39.1	4.5 ± 0.1	2.4 ± 0.1	0.12 ± 0.03
1.0	5.7	19.3	2.4 ± 0.1	1.8 ± 0.1	0.24 ± 0.03	55.3	2.8 ± 0.1	2.1 ± 0.1	0.10 ± 0.03
0.5	4.0	27.3	1.4 ± 0.1	1.5 ± 0.1	0.17 ± 0.03	78.3	1.4 ± 0.1	1.5 ± 0.1	0.07 ± 0.03
0.3	3.1	35.3	0.7 ± 0.1	1.0 ± 0.2	0.14 ± 0.03	101.0	N/A	N/A	N/A
				Dimond shaped (2.3)					
2.0	4.3	25.3	3.5 ± 0.2	1.8 ± 0.1	0.23 ± 0.03	72.5	3.9 ± 0.2	2.1 ± 0.1	0.08 ± 0.03
1.0	3.1	35.8	3.1 ± 0.2	2.3 ± 0.2	0.15 ± 0.03	102.5	N/A	N/A	N/A
0.5	2.2	50.6	3.1 ± 0.2	3.2 ± 0.2	0.10 ± 0.03	144.9	N/A	N/A	N/A

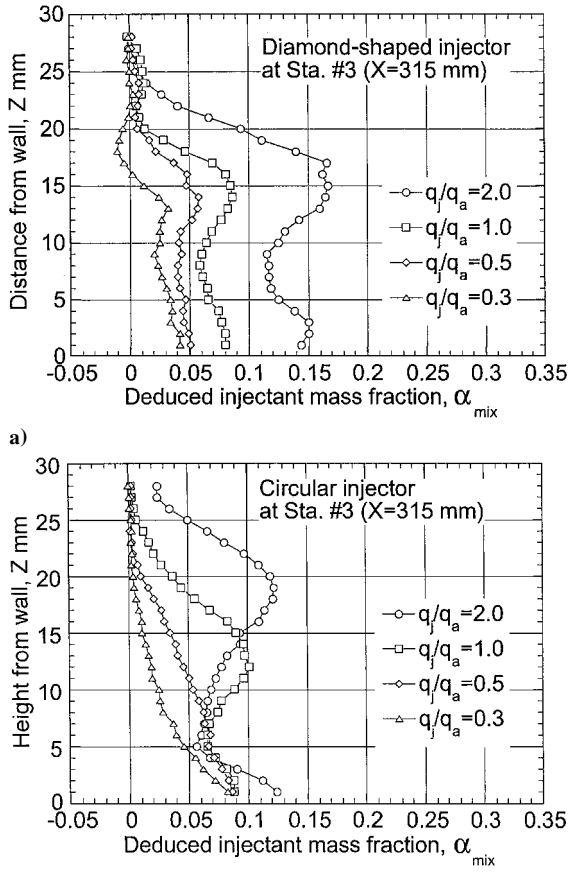

Fig. 10 Deduced injectant mass fraction (α_{mix}) distributions on contour symmetry plane at station 3 (X = 315 mm) with a) diamond-shaped injector and b) circular injector.

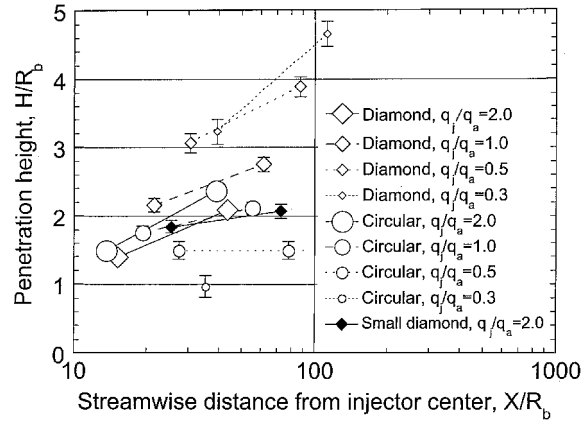

Fig. 11 Summary of penetration height data with different shaped injectors.

where G_j is the injectant mass flow rate. This length scale clearly takes the injectant flow rate into account, and both the streamwise distances between the injector and the probing location X and the penetration heights are normalized with R_b in Table 1. At lower dynamic pressure ratios, the penetration height of the jet plume through the diamond-shaped injector was superior to that through the circular injector. However, the penetration heights became comparable at higher dynamic pressure ratios. Using the wedge-shaped orifice (with a wedge-shaped front half and a round-shaped back half), Barber et al.[5] reported about 50% larger penetration than that through a circular injector at station 1 with sonic helium injection. Their injection conditions were almost identical to the current ones with $q_j/q_a = 0.3$. With the diamond-shaped injector, the normalized penetration height was about 200% larger than with the circular injector at this dynamic pressure ratio, showing the better performance of the diamond-shaped injector in comparison to that of the earlier wedge-shaped injector.

Figure 11 summarizes all of the penetration height data with different shaped injectors at different streamwise locations. Both the penetration height and the sampling location were normalized with R_b. At a fixed X/R_b of 40, the normalized penetration height of the jet plume through the diamond-shaped injector was greater with smaller dynamic pressure ratio, showing the benefits of lower dynamic pressure injection. Thus, one should use a larger diamond-shaped injector orifice with lower dynamic pressure under a constraint on total flow rate.

In Fig. 11, the data obtained with the diamond-shaped injector show almost identical growth rates of penetration regardless of the dynamic pressure, whereas the penetration growth rates with the circular injector decreased with a reduction in the dynamic pressure ratio. Thus, the superiority of the lower dynamic ratio injection in cases with the diamond-shaped injector was maintained over a wide range of streamwise locations (X/R_b). In the case with the diamond-shaped injector, lower dynamic pressure resulted in weaker interaction between the jet and the freestream associated with less total pressure loss of the plume, and higher dynamic pressure resulted in a generation of more intensive streamwise vortices. Thus, the penetration growth rate remained almost constant regardless of the dynamic pressure ratio.

Figure 12 summarizes the maximum deduced mass fraction decay with different shaped injectors. Again, the sampling location was

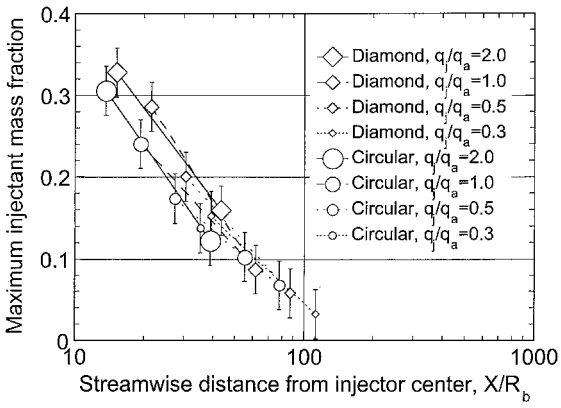

Fig. 12 Maximum deduced concentration decay with different shaped injectors.

normalized with R_b. For the maximum mass fraction decay, the data with both the diamond-shaped and circular injectors showed almost identical behavior within the accuracy (±3%) of the present measurement technique. Though the jet plume through the diamond-shaped orifice penetrated further into the freestream, the mixing process of the jet with the surrounding air was insensitive to the injector orifice shape.

Effects of Injector Orifice Size

As mentioned before, injection from a larger injector orifice with lower dynamic pressure would result in a larger absolute penetration height for the same mass flow rate. However, the effects of boundary-layer thickness on the penetration compared to those of the injector orifice size should also be addressed. Data with the smaller diamond-shaped injector are also summarized in Table 1. Note that we could not detect the core of the plume above the boundary layer at station 3 with lower pressure injection ($q_j/q_a \leq 1$).

Penetration data for the smaller diamond-shaped injector at $q_j/q_a = 2.0$ are also plotted in Fig. 11. The penetration heights and growth rate were almost identical to those with the larger diamond-shaped injector at $q_j/q_a = 2.0$, showing that the effects of boundary-layer thickness on the penetration data were negligible in the present range of scales.

Because the area of the large injector orifice was three times that of the small injector, the dynamic pressure ratio should be one-third for the same flow rate. The effective radius ($R_b = 2.8$ mm) in the case with the large injector at $q_j/q_a = 0.3$ is almost identical to those with the small injector at $q_j/q_a = 1$ ($R_b = 3.1$ mm). The plume from the large injector penetrated 20–30% farther into the freestream, confirming the benefits of using a larger injector with a lower dynamic pressure ratio. On the other hand, the maximum concentrations were almost identical in both cases, supporting the results in Fig. 12.

Angled Injection at High Dynamic Pressure Ratio

As noted earlier, the jet through the diamond-shaped injector became a large obstacle and blocked the freestream at high dynamic pressures, which caused a separation ahead of the jet. Adding sweepback angle can be expected to mitigate this separation and intensive interactions between the jet and the freestream to intensify the streamwise vortices and to increase penetration. Thus, the effects of the sweepback angle on penetration, mixing, and vortices generation were investigated with an injector without yaw angle at the dynamic pressure ratio of 2.0. Effects of adding yaw angle to a sweptback injector on penetration, mixing, and vortices generation were also investigated in hopes of creating further intensive streamwise vortices.

Flow Visualization

Figures 13a–13c show oil-flow surface patterns around the orifices with sweepback angles of 0, 30, and 60 deg, respectively,

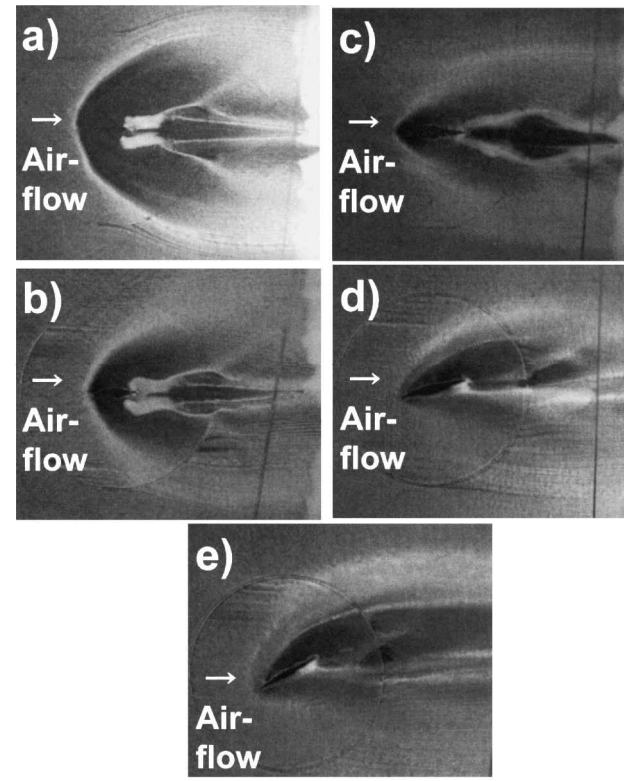

Fig. 13 Oil-flow visualization of surface flow with a) 0-, b) 30-, and c) 60-deg sweepback angle without yaw angle and with d) 15- and e) 30-deg yaw angle and 60-deg sweepback angle.

whereas Figs. 13d and 13e show the flow around the 60-deg sweptback orifices with yaw angles of 15 and 30 deg, respectively. In Figs. 13, the freestream is from left to right. Without sweepback angle, a separation was observed ahead of the orifice (Fig. 13a). At this highly underexpanded condition, the jet expanded rapidly in the spanwise direction and became a large obstacle to the freestream. The trace of the bow shock in Fig. 13a shows the intensive interaction between the jet and the freestream. With 30 deg of sweepback angle (Fig. 13b), the separation was mitigated, and the bow shock was weakened. With 60 deg of sweepback angle (Fig. 13c), the bow shock was further weakened, and the separation vanished. This result implies lesser total pressure loss in the freestream at larger sweepback angle.

The complicated flow pattern in the jet wake is due to the induction of a pair of streamwise vortices. Triangular accumulations of oil show the origin of the pair of streamwise vortices, which then traveled downstream. The structure of the wake flow was qualitatively identical regardless the sweepback angle, though the traces suggest more intensive induction of vortices with less sweepback angle.

With 15 deg of yaw angle added to the 60-deg sweptback orifice (Fig. 13d), an intensive bow shock was observed on the compression side of the jet, whereas no apparent separation was observed. The bow shock on the suction side of the jet became almost invisible. Also observed was a reverse flow from the compression-side to the suction-side around the trailing edge of the orifice. This shows a large difference in pressure between the two sides. The pattern in the wake of the jet, which shows the origin of the streamwise vortices, became asymmetric, whereas the location and the extent of the pattern was almost identical to those without yaw angle. With 30 deg of yaw angle added to the 60-deg sweptback orifice (Fig. 13e), the bow shock on the compression side of the jet became quite strong, and a separation was observed ahead of the jet, showing intensive interaction between the jet and the freestream. The wave from the leading edge of the jet on the suction side was quite weak, though it originated at the separation ahead of the jet. The reverse flow around the trailing edge of the orifice was visible. The pattern in the wake

of the jet became more asymmetric and originated closer to the jet than that in the case with a 15-deg yaw angle.

Injectant Contours

Figures 14a and 14b show contours of deduced injectant mass fraction and the enthalpy deficit factor, respectively, at station 1, with a sweepback angle of 60 deg and without a yaw angle. The location of the plume center (where the injectant concentration is maximum) is shown with an "×" in Fig. 14a. By assuming an oval shape of the vorticity effect extent (dashed line in Fig. 14b), we can also evaluate the penetration height of the streamwise vortices as the center (shown with "×" in Fig. 14b) of the oval shape. A constriction of the injectant contour occurred at around the outer boundary of the vorticity effect extent, showing an interaction between the jet and the streamwise vortices. This interaction became more intensive with sweepback angle, and the plume was divided into two: one part above the boundary layer and another part within the boundary layer, in Fig. 14a. Fine-scale mixing should be more intensive with larger sweepback angles because of more intensive interaction between the plume and the streamwise vortices.

Figures 15a and 15b show contours of deduced injectant mass fraction and the enthalpy deficit factor, respectively, at station 1, with a sweepback angle of 60 deg and a 15-deg yaw angle. The locations of both the plume center and the vorticity effect extent center are shown in Figs. 15. The injectant contours still show mushroomlike, but asymmetric, shapes. Note that the plume without yaw angle (Fig. 14a) was divided into two parts, one in the freestream and the other in the boundary layer, whereas that with yaw angle left no high concentration portion within the boundary layer. With 15 deg of yaw angle, the plume penetrated farther than that without yaw angle.

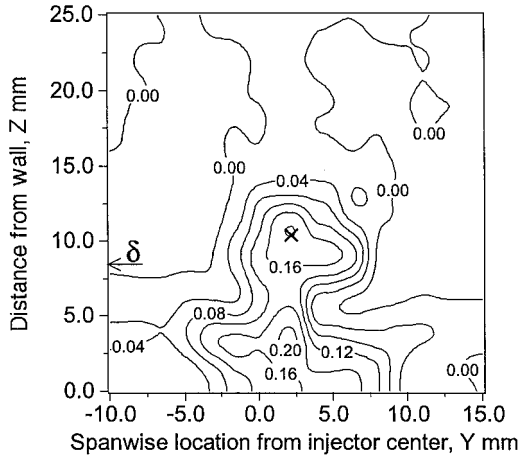

a)

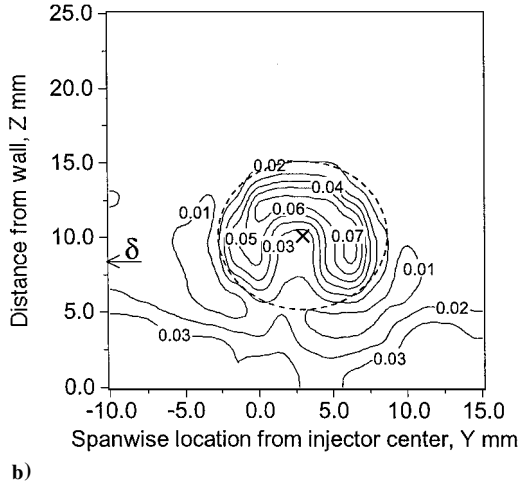

b)

Fig. 14 Contours of a) deduced injectant mass fraction (α_{mix}) and b) enthalpy deficit factor at station 1 (X = 110 mm) with 60-deg sweepback angle without yaw angle.

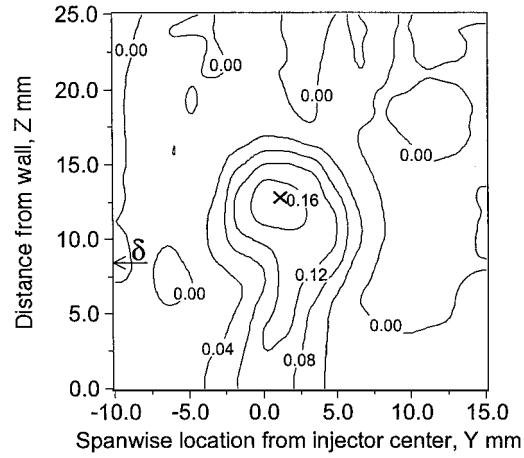

a)

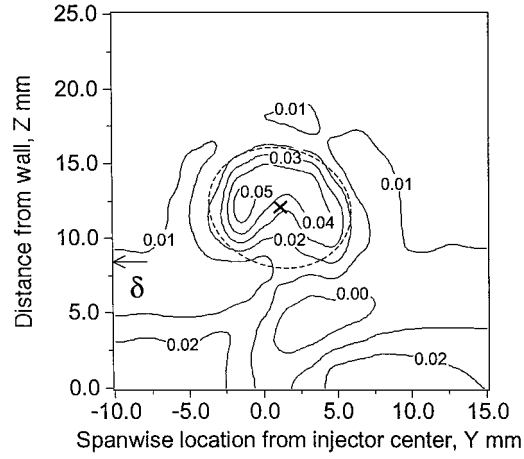

b)

Fig. 15 Contours of a) deduced injectant mass fraction (α_{mix}) and b) enthalpy deficit factor at station 1 (X = 110 mm) with 60-deg sweepback angle and 15-deg yaw angle.

With nonzero yaw angle, the vorticity effect extent became shrunken in extent and weaker in the maximum deficit factor. The center of the vorticity effect extent also penetrated farther with a 15-deg yaw angle.

For non-yaw-angled orifices, the measurements were done at both stations 1 and 3, whereas these were done at only station 1 for the yaw-angled orifices. All penetration height data of the plume, as well as those of the center of the vorticity effect extent, are summarized in Table 2.

Plume Penetration and Mixing of Nonyawed Orifices

Figure 16 shows the penetration height and penetration growth rate for different sweepback angles without yaw angle. At both stations, the penetration height increased with sweepback angle. The growth rate is larger with larger sweepback angle, showing the effectiveness of the angled injection.

As shown in Table 2, the vorticity effect extent penetrated farther than the plume itself at station 3, showing that the penetration of the vortices played a key role on the plume penetration by rolling up the plume. However, the penetration of the vorticity extents were almost identical to that of the plume at station 1, and initial penetration of the jet plume is still influential on the penetration of the plume at this streamwise location. The extrapolation of the data in Fig. 16 implied that even the initial penetration of the plume (around X–0) was larger with larger sweepback angle, which is contrary to the observation of Gruber et al.[6] for an elliptical injector. Their observation was limited to a very close field to the injector ($X/D_j < 5$), so that we need a detailed observation in the region downstream of their observation sight. A possible explanation is a difference in

Table 2 Summary of penetration height and maximum injectant mass fraction of the jet plume with angled injection

				Station 1				Station 3			
Sweep-back	Yaw angle	D_{eff}, mm	R_b, mm	X/R_b	H/R_b	H_{VC}/R_b	$\alpha_{\max}$	X/R_b	H/R_b	H_{VC}/R_b	$\alpha_{\max}$
0	0	2.3	2.3	25.3	1.8 ± 0.1	1.8 ± 0.1	0.23 ± 0.03	72.5	2.1 ± 0.1	2.9 ± 0.1	0.08 ± 0.03
30	0	2.4	2.4	23.7	2.2 ± 0.1	1.9 ± 0.1	0.21 ± 0.03	67.8	2.6 ± 0.1	3.3 ± 0.1	0.07 ± 0.03
60	0	2.1	2.1	27.0	2.7 ± 0.1	2.5 ± 0.1	0.22 ± 0.03	77.2	3.7 ± 0.1	4.4 ± 0.1	0.06 ± 0.03
60	15	2.1	2.1	27.0	3.2 ± 0.1	2.9 ± 0.1	0.18 ± 0.03	77.2	——	——	——
60	30	2.1	2.1	27.0	1.7 ± 0.1	2.5 ± 0.1	0.26 ± 0.03	77.2	——	——	——

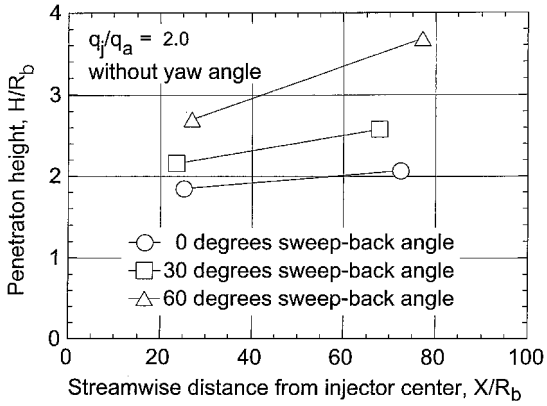

Fig. 16 Summary of penetration height data with different sweepback angles without yaw angle.

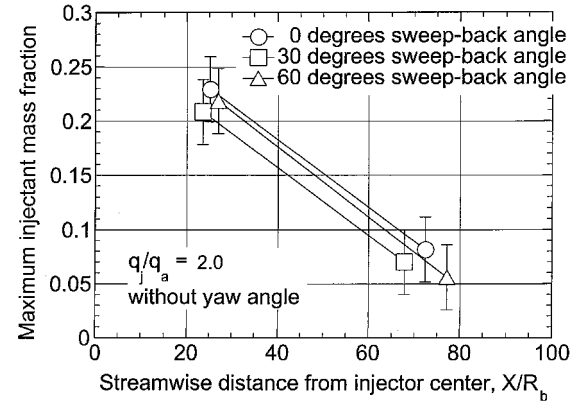

Fig. 17 Summary of maximum injectant concentration data with different sweepback angles without yaw angle.

shock formation within the plume, which governs the total pressure loss of the plume. In the case with larger sweepback angle, the less intensive interactions between the jet and the freestream might cause less total pressure loss of the plume, so that the plume might continue to penetrate further than that through the lesser sweepback angled injector, even though the perpendicular component of the jet momentum was less. This less intensive interaction might also result in less total pressure loss in the freestream.

McClinton[7] reported that giving 30 and 60 deg of sweepback angle to a circular injector resulted in a 30–40% and 50–70% gain in penetration height, respectively. Note that his freestream conditions, including Mach number ($M_a = 4$), the injectant species (hydrogen), and the jet-to-freestream dynamic pressure ratio ($q_j/q_a = 1$) were different from those in the present study. Neither the penetration height of the jet through the circular injector with sweepback angle,[8,10] nor that of the perpendicular jet through the diamond-shaped injector, were correlated well with the dynamic pressure ratio, so that we could not filter out the effects of the difference in the dynamic pressure ratio, and direct comparison with the penetration height in Ref. 7 was not possible. In the present study, giving 30 and 60 deg of sweepback angle to the diamond-shaped injector resulted in 20–30% and 50–70% gain in penetration height, respectively, so that giving a 60 deg sweepback angle to the diamond-shaped orifice was as effective as the case with the circular injector, especially at locations farther downstream.

Figure 17 shows the maximum deduced injectant concentration and its decay with different sweepback angles. The maximum concentration is lowest with the 30-deg sweepback angle. However, the variation of the maximum concentration with the sweepback angle is in the range of the expected uncertainty (±3% in injectant mass concentration) of the measurement technique in the present study, and the effects of sweepback angle on the maximum concentration could not be addressed in this range.

Plume Penetration and Mixing of Yawed Orifices

Figure 18 shows the penetration height and the maximum deduced injectant concentration at station 1 as a function of injector yaw angle. The jet penetration height had a maximum around a yaw angle of 15 deg, and a farther increase in yaw angle resulted in a drastic decrease in the penetration height.

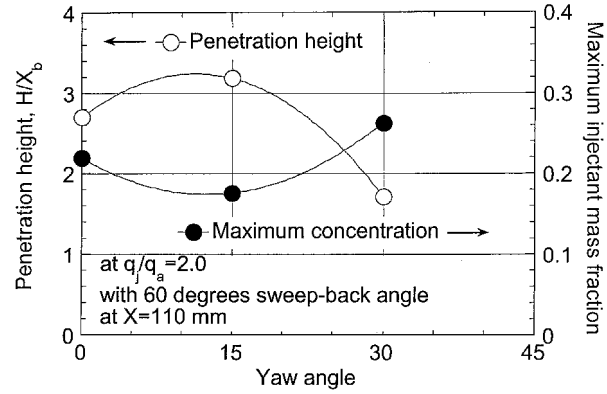

Fig. 18 Summary of penetration height and maximum injectant concentration data at station 1 (X = 110 mm) with 60-deg sweepback angle and different yaw angles.

As shown in Table 2, the large penetration of the plume was due to the large penetration of the streamwise vortices in the case with 15 deg of yaw angle. Thus, like the earlier discussion about data in the case without yaw angle, a larger penetration of the vortices resulted in a larger penetration of the plume, showing the effectiveness of the streamwise vortices on the rolling up of the plume. The larger penetration of the streamwise vortices was due to the pressure difference between the compression-side and the suction-side of the jet, which caused a spanwise flow along the wall, which might roll up the whole flowfield, including the induced streamwise vortices.

The streamwise vortices in the case with 30 deg of yaw angle penetrated farther than those in the case without yaw angle, but less than those in the case with 15 deg of yaw angle. Furthermore, the center of the plume penetrated much less than the center of the vorticity effect extent in this case. Flow visualization showed that a separation occurred ahead of the jet with this configuration, and this interaction between the jet and freestream suppressed the initial penetration of the jet. Consequently, the jet inclined toward the wall, pushing the induced streamwise vortices toward the wall to reduce their penetration.

The maximum concentration was lowest at a yaw angle of 15 deg, and it increased considerably with a yaw angle of 30 deg. The

favorable interaction between the plume and the streamwise vortices enhanced the mixing at a yaw angle of 15 deg. On the other hand, the interaction between the jet and the freestream (namely, the occurrence of the separation) especially suppressed the penetration of the jet plume, and the interaction between the plume and the vortices was weakened as these centers were separated for the yaw angle of the 30-deg case.

The increase in the penetration height by adding 15 deg of yaw angle was not observed in the case of circular injectors, in which both the penetration height and the maximum concentration were almost identical regardless of the yaw angle.[10] In the case with a circular injector, a separation region was observed around the trailing edge of the orifice.[10] This separation region mitigated the pressure difference between the compression-side and the suction-side and, thus, the rolling up of the streamwise vortices. As a result, the penetration of the streamwise vortices and, hence, that of the plume, became less sensitive to the yaw angle than in the case with a diamond-shaped orifice.

Giving 15 deg of yaw angle resulted in the more intensive interaction between the jet and the freestream, as shown in Fig. 15d, which might result in a larger total pressure loss. However, in the case with a circular injector,[10] giving even 28 deg of yaw angle to a 60-deg sweptback injector caused no significant increase in total pressure loss. Thus, the penalty of giving 15 deg of yaw angle to the 60-deg sweptback diamond-shaped injector, in terms of total pressure loss, would be minimal, and the injector should have the best performance among all injectors tested in the present study at the dynamic pressure ratio of 2.0.

Conclusions

The penetration and mixing of the plume from diamond-shaped injector orifices in a Mach 3 crossflow was examined experimentally in a blowdown-type tunnel facility. Visualizations of the flowfield were done to understand the behavior of the plume near the injectors. Aerothermodynamic probing measurements were done at downstream stations to evaluate the penetration and mixing of the plume, and a modified mixing analogy was used for deduction of equivalent concentration from temperature measurement data.

For the perpendicular injection, the effect of injection pressure was investigated, and a circular injector with an identical equivalent diameter was also tested as a reference. The main conclusions are as follows:

1) The jet plume from the diamond-shaped injector with high-pressure ratios expanded mainly in the spanwise direction. This expansion resulted in a disruption of the original sharp plume shape resulting in more intensive interaction with the freestream for higher-pressure injection. However, this interaction caused streamwise vortices to enhance mixing.

2) The jet plume from the diamond-shaped injector showed larger penetration and penetration growth rate at lower dynamic pressure ratios compared to that from the circular injector. It also showed larger penetration than that from a wedge-shaped injector in Ref. 5 at low dynamic pressure ratios.

3) The maximum deduced injectant mass fraction decay rates were almost identical, regardless of the injector configuration and the dynamic pressure ratio.

4) The effects of the injector orifice size were examined, and the effects of the boundary-layer thickness compared to the injector size were found to be negligible in the range studied.

5) For the diamond-shaped injector, injection from a larger injector with lower dynamic pressure ratio is recommended for a given injectant mass flow rate.

To increase the penetration height at high-pressure injection, both sweepback angle and yaw angle were given to the diamond-shaped injector. The main conclusions are as follows:

1) The plume from the nonyawed injector with larger sweepback angles penetrated further, with a slightly larger growth rate of the penetration height. The penetration of the streamwise vortices played a key role on the enhancement of the plume penetration.

2) The maximum deduced injectant mass fraction was essentially insensitive to the sweepback angle for the nonyawed injectors within the accuracy of the present measurement technique.

3) Adding sweepback angle to the diamond-shaped injector was as effective as it was for a circular injector in enhancing the penetration height of the plume.

4) The penetration of the plume increased drastically by adding 15 deg of yaw angle to the diamond-shaped injector with 60 deg of sweepback angle. The pressure difference between the compression-side and the suction-side of the plume enhanced the penetration height of the induced streamwise vortices and, consequently, that of the plume. This effect had not been observed in the cases with a circular orifice.

5) Further yaw-angle increase caused separation ahead of the plume, and the interaction between the freestream and the jet reduced the penetration of the plume substantially.

Acknowledgments

The authors would like to thank G. Stafford, B. Stanger, K. Morris, and G. Dudding of the Aerospace and Ocean Engineering Department at Virginia Polytechnic Institute and State University for their valuable support of the present research.

References

[1]Schetz, J. A., Thomas, R. H., and Billig, F. S., "Mixing of Transverse Jets and Wall Jets in Supersonic Flow," *Separated Flows and Jets*, edited by V. V. Kozlov and A. V. Dovgal, Springer-Verlag, Berlin, 1991, pp. 807–837.

[2]Hollo, S. D., McDaniel, J. C., and Hartfield, R. J. Jr., "Quantitative Investigation of Compressible Mixing: Staged Traverse Injection into Mach 2 Flow," *AIAA Journal*, Vol. 32, No. 3, 1994, pp. 528–534.

[3]Fuller, R. P., Wu, P.-K., Nejad, A. S., and Schetz, J. A., "Comparison of Physical and Aerodynamic Ramps as Fuel Injectors in Supersonic Flow," *Journal of Propulsion and Power*, Vol. 14, No. 2, 1998, pp. 135–145.

[4]Jacobsen, L. S., Schetz, J. A., and Ng, W. F., "Flowfield Near a Multiport Injector Array in a Supersonic Flow," *Journal of Propulsion and Power*, Vol. 16, No. 2, 2000, pp. 216–226.

[5]Barber, M. J., Schetz, J. A., and Roe, L. A., "Normal, Sonic Helium Injection Through a Wedge-Shaped Orifice into Supersonic Flow," *Journal of Propulsion and Power*, Vol. 13, No. 2, 1997, pp. 257–263.

[6]Gruber, M. R., Nejad, A. S., Chen, T. H., and Dutton, J. C., "Mixing and Penetration Studies of Sonic Jets in a Mach 2 Freestream," *Journal of Propulsion and Power*, Vol. 11, No. 2, 1995, pp. 315–323.

[7]McClinton, C. R., "The Effects of Injection Angle on the Interaction Between Sonic Secondary Jets and a Supersonic Free Stream," NASA TN D-6669, 1972.

[8]Mays, R. B., Thomas, R. H., and Schetz, J. A., "Low Angle Injection into Supersonic Flow," AIAA Paper 89-2461, July 1989.

[9]Cohen, L. S., Coulter, L. J., and Egan, W. J., Jr., "Penetration and Mixing of Multiple Gas Jets Subjected to a Crossflow," *AIAA Journal*, Vol. 9, No. 4, 1971, pp. 718–724.

[10]Fuller, E. J., Mays, R. B., Thomas, R. H., and Schetz, J. A., "Mixing Studies of Helium in Air at High Supersonic Speeds," *AIAA Journal*, Vol. 30, No. 9, 1992, pp. 2234–2243.

[11]Shimura, T., "Load Oscillations due to Unstart of Hypersonic Engines," Paper 98-a-1-28, 1998.

[12]Tomioka, S., Jacobsen, L. S., and Schetz, J. A., "Modified Mixing Analogy for Studies of Jet Mixing in Supersonic Flows," *Journal of Propulsion and Power*; also AIAA Paper 2000-0088, Jan. 2000.

[13]Volluz, R. J., "Handbook of Supersonic Aerodynamics, Section 20 — Wind Tunnel Instrumentation and Operation," Bureau of Ordnance, Dept. of Navy, NAVORD Rept. 1488, Ordnance Aerophysics Lab., Daingerfield, Texas, Vol. 6, 1961.

[14]Schadow, K. C., Gutmark, E., Koshigoe, S., and Wilson, K. J., "Combustion-Related Shear-Flow Dynamics in Elliptical Supersonic Jets," *AIAA Journal*, Vol. 27, No. 10, 1989, pp. 1347–1353.

[15]Schadow, K. C., Gutmark, E., Wilson, K. J., and Parr, D. M., " Mixing Characteristics of a Ducted Elliptical Jet," *Journal of Propulsion and Power*, Vol. 4, No. 4, 1988, pp. 328–333.

[16]Billig, F. S., Orth, R. C., and Lasky, M., "Unified Analysis of Gaseous Jet Penetration," *AIAA Journal*, Vol. 9, No. 6, 1971, pp. 1048–1058.

[17]Gruber, M. R., Nejad, A. S., Chen, T. H., and Dutton, J. C., "Compressibility Effects in Supersonic Transverse Injection Flowfield," *Physics of Fluids*, Vol. 9, No. 5, 1997, pp. 1448–1461.

[18]Schetz, J. A., "Interaction Shock Shape for Transverse Injection in Supersonic Flow," *Journal of Spacecraft and Rockets*, Vol. 7, No. 2, 1970, pp. 143–149.